

1 **Field performance of four vibrating-wire piezometer installation methods**

2 Nathan Young^{1*}, Jean-Michel Lemieux¹, Laura Mony¹, Alexandra Germain¹, Pascal
3 Locat², Denis Demers², Ariane Locat³, Serge Leroueil³, Jacques Locat¹

4 1. Département de géologie et de génie géologique, 1065 avenue de la Médecine,
5 Université Laval, Québec (Québec), Canada, G1V 0A6.

6 2. Section des mouvements de terrain, Direction de la géotechnique et de la
7 géologie, Ministère des Transports du Québec, Québec, (Québec), Canada

8 3. Département de génie civil et des eaux, 1065 avenue de la Médecine, Université
9 Laval, Québec (Québec), Canada, G1V 0A6.

10 *Corresponding author. +1 418-656-7679, jmlemieux@ggl.ulaval.ca

11 For submission to J. Geotech. Geoenviron. Eng.

12 **Abstract**

13 Vibrating wire piezometers provide a number of advantages over the traditional
14 hydraulic piezometer design. There are many methods and configurations for installing
15 vibrating-wire piezometers, with the most common being: single piezometers in sand
16 packs (SP), multilevel piezometers in sand packs (MLSP), and fully-grouted multilevel
17 piezometers using either bentonite (FGB) or cement-bentonite grout (FGCB). This study
18 assesses the performance of these four different installation methods for vibrating wire
19 piezometers at a field site possessing complex stratigraphy, including glacial and marine
20 sediments. Pore pressure data recorded between December 2017 and July 2019 were
21 analyzed to accomplish this objective. Data indicate that SP, MLSP, and FGB
22 piezometers performed well. This determination is based on the fact that piezometers
23 installed at the same depth with these arrangements recorded similar pressure variations

24 that were coherent with the hydrogeological setting. Of the two fully-grouted installations
25 using cement-bentonite grout, one installation failed completely due to a hydraulic short
26 circuit, caused either by shrinkage of the grout or flow occurring along the wires of the
27 embedded instruments. While the FGB-type piezometers used in this study worked
28 correctly, the lack of standard methods concerning both the construction of fully-grouted
29 piezometers is concerning. Furthermore, the lack of a standard method for mixing
30 cement-bentonite grout likely contributed to the failure of the FGCB installations. Thus,
31 due to the lack of guidance for both construction and grout preparation, the use of a
32 bentonite grout removes a degree of uncertainty when fully-grouted installation
33 techniques are used.

34 RÉSUMÉ

35 **Keywords:**

36 **1 Introduction**

37 In the province of Quebec, 89% of the population lives within the extent of the
38 Champlain Sea formations, which were deposited by seawater invasion after the
39 Wisconsin glaciation and are prone to landslides (Demers et al. 2014). In response to the
40 landslide risk posed by these formations, the Quebec Ministry of Transport (MTQ) has
41 deployed an extensive network of vibrating-wire piezometers (VWP) to monitor spatial
42 and temporal variation of pore pressures in clay slopes (Cloutier et al. 2017). This type of
43 piezometer provides a number of advantages over the traditional hydraulic piezometer
44 design, very small amounts of liquid are required for measurement; measurement
45 accuracy is very high; response times to changes in water pressure are very quick; and it

46 is possible to transmit observed responses over long distances (McKenna, 1995).
47 However, the largest advantage of using of VWP is the ability to deploy multiple
48 instruments within a single borehole. These multilevel VWP installations are created by
49 mounting several piezometers to a single grout tube, allowing for multiple depths to be
50 instrumented quickly and inexpensively.

51 Currently, there are many methods of constructing multilevel VWP installations,
52 however the most common are multilevel piezometers in sand packs, and fully-grouted
53 multilevel piezometers using either bentonite or cement-bentonite grout. Historically, the
54 most common method for installing a vibrating-wire piezometer involves encasing a
55 single instrument within a sand pack (referred to as the SP method, hereafter), which is
56 then sealed above and below the measurement interval by layers of bentonite (Obbink,
57 1969; Anochikwa et al. 2011). Piezometers installed in this manner can either be installed
58 as a single instrument, or multiple sand pack/bentonite caps can be utilized within a
59 single borehole (i.e., multilevel VWPs with sand packs, MLSP; Germain et al.
60 *Submitted*). While the use of sand packs has long been the standard method for
61 installation, concerns over cost, as well as the long-term integrity of sand packs and
62 bentonite caps have resulted in fully-grouted methods becoming increasingly popular in
63 recent years (Simeoni, 2012; Marefat et. 2018).

64 Fully-grouted methods result in a piezometer that is completely encased by either
65 bentonite or cement-bentonite grout, and does not include a sand pack (Mikkelsen, 2002).
66 When these methods are used, the VWPs are first attached to a grout pipe that is then
67 lowered into the base of the borehole. Grout is then pumped through the pipe, completely
68 filling the borehole and encasing the piezometers (Contreras et al. 2008). Advocates of

69 this approach cite faster installation times and a lower potential for water to be routed to
70 the piezometer from above or below the targeted installation depth (i.e., “short-
71 circuiting”; McKenna, 1995). Furthermore, the ability to mount multiple instruments to a
72 single grout pipe allows for a nest of VWPs to installed in the absence of a sequence of
73 bentonite seals and sand packs (Mikkelsen and Green, 2003).

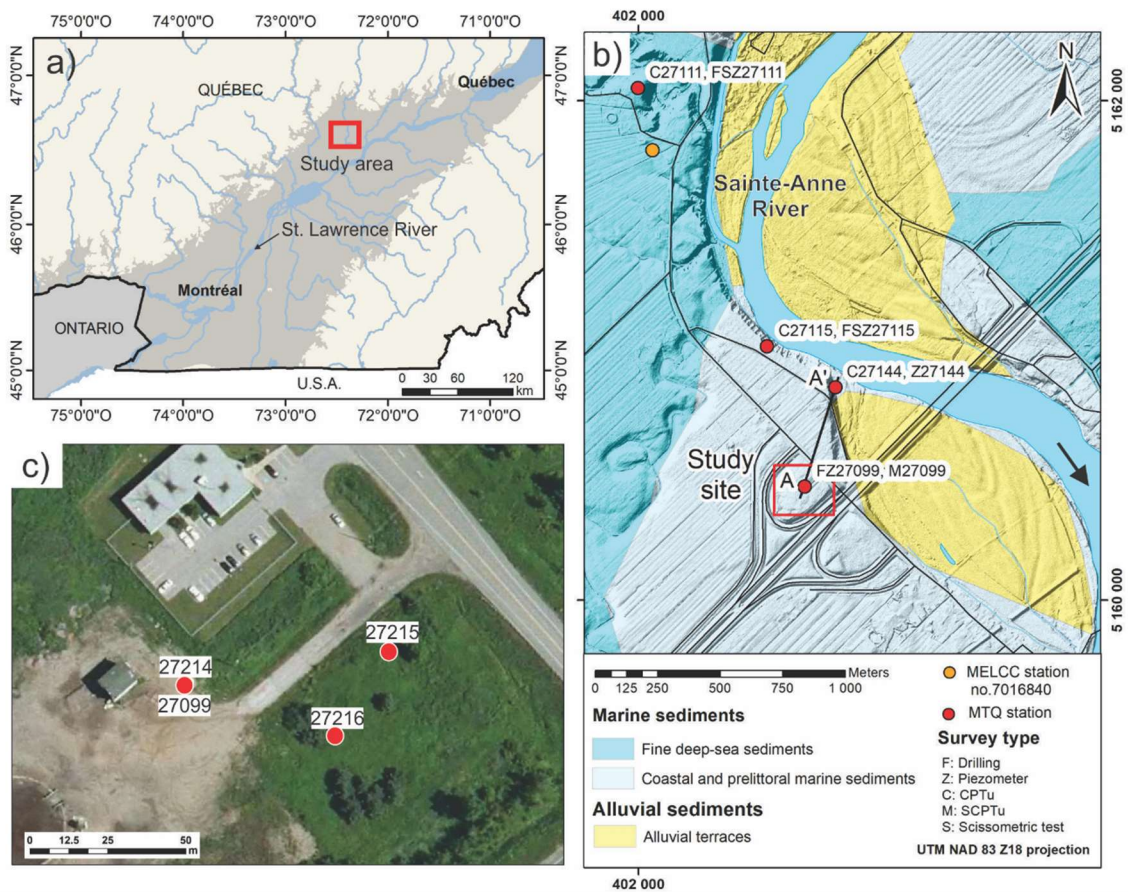
74 While fully-grouted methods have distinct advantages, there are potential drawbacks
75 which have not been thoroughly explored. Specifically, fully-grouted methods require
76 precise preparation of the grout mixture, and the grout hydraulic conductivity (K) needs
77 to be calibrated to ensure that it is at least 2-3 orders of magnitude lower than the
78 surrounding formation (McKenna, 1995). Improperly mixed grout may crack during
79 curing, resulting in short circuiting. Meanwhile, grout that is too permeable relative to the
80 surrounding formation can cause measurement errors (Marefat et al. 2018). While each
81 installation method has associated risks and advantages, their comparative performance
82 has not been extensively documented in the scientific literature.

83 This study focuses on how different installation methods impact the long-term
84 reliability of multilevel piezometer installations, as well as the accuracy of the
85 observations they produce (i.e., the performance of each installation). Specifically, this
86 work was performed to assess the risks and benefits of using either sand packs or fully-
87 grouted methods. As such, the objective of this study is to (1) assess the performance of
88 different methods for constructing multilevel VWP installations at a field site possessing
89 a complex stratigraphy, and (2) to recommend the most suitable methods for installing
90 and configuring an observation network for monitoring groundwater conditions. To
91 accomplish this goal, multilevel VWP installations were constructed at a field site in the

92 municipality of Sainte-Anne-de-la-Pérade (Québec, Canada) using four different
 93 methods. The results of these multilevel installations were then compared to a reference
 94 dataset, gathered from individual vibrating-wire piezometers in sand packs (SP). An
 95 analysis of pore pressure data recorded between December 2017 and July 2019 was then
 96 conducted to compare the performance of the different piezometers.

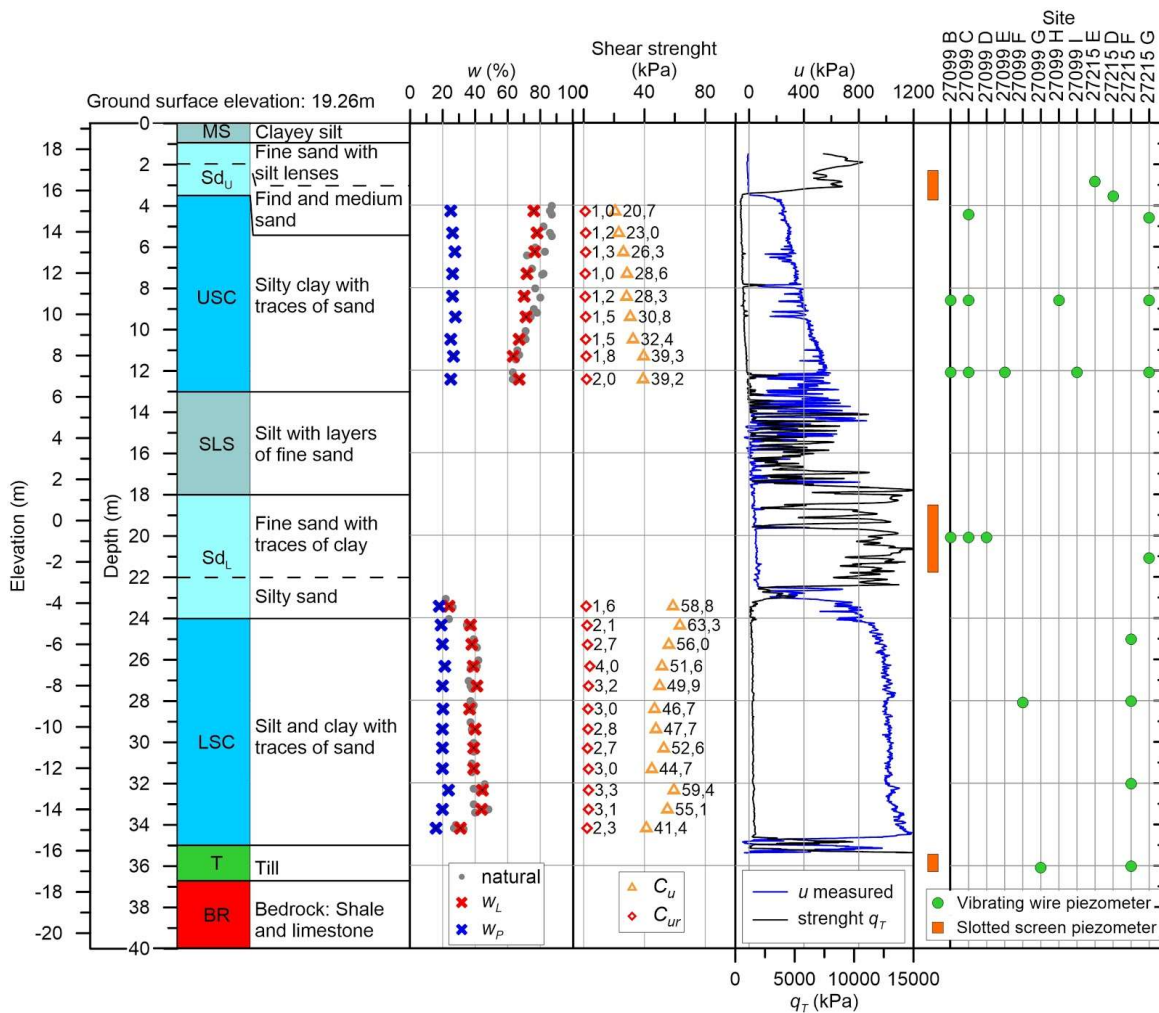
97 **2 Study area**

98 The study site is located close to St-Anne-de-la-Pérade, about 100 km west of Quebec
 99 City, on the north shore of the St-Lawrence River in the Province of Quebec, Canada
 100 (Figure 1).



102 Figure 1. a) Site location within the St. Lawrence Lowlands basin, showing the area
103 invaded by Champlain Sea (dark gray). b) Digital elevation model overlain with the
104 surficial geology of the study area. The location of the study site is shown within the red
105 box. c) Map of the study site showing the location of the monitoring instrumentation used
106 in this study.

107 The study area is located within the St. Lawrence Lowlands basin, and the bedrock
108 unit present at the study site, the Utica Shale, is composed of calcareous shale and clayey
109 limestone. Sitting atop the shale is a 35-m thick complex succession of marine sediments
110 as the area was invaded by the Champlain Sea following the last glacial maximum. This
111 sequence constitutes a clay plain that is locally covered by littoral sediments (Figure 2).
112 More modern sedimentary deposits can be found along the Sainte-Anne rivercourse, and
113 the river is deeply incised within its current channel.

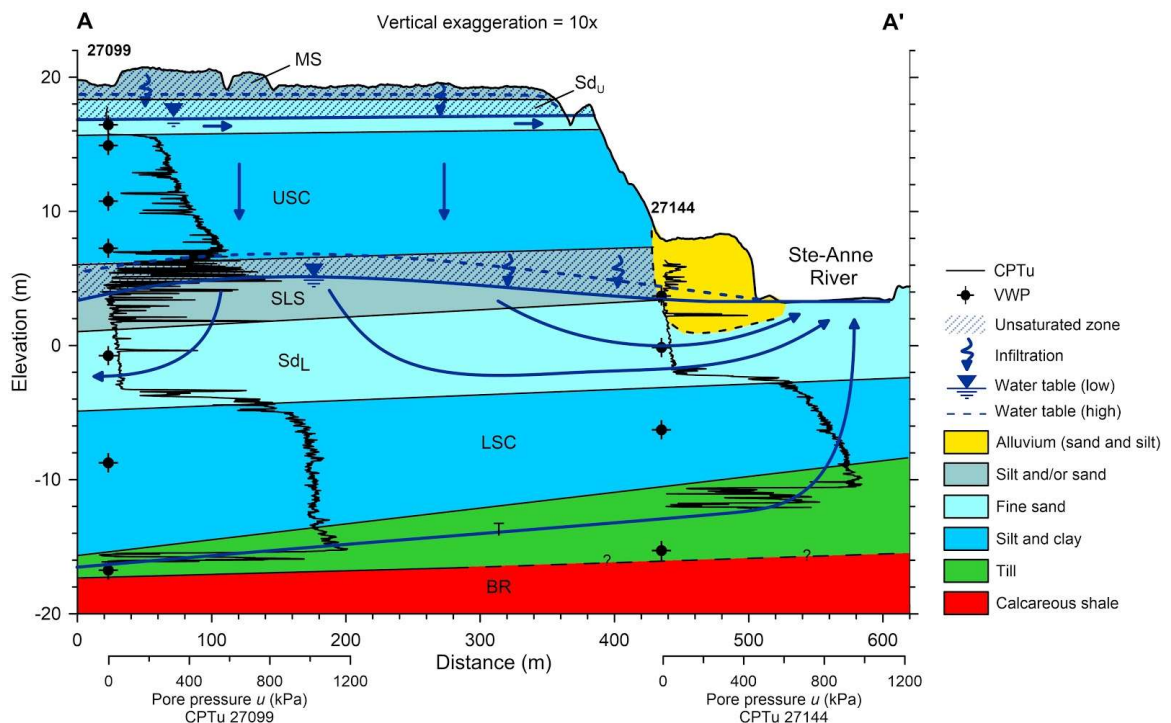


115
 116 Figure 2: Geotechnical profile at location 27214 (located on Figure 1c) showing site
 117 stratigraphy, liquid and plastic limits, undrained shear strength, pore pressure and
 118 corrected tip resistance from CPTu and piezometers depth.

119 The sedimentary units present on site begin with a 2-m-thick layer of till (T), followed by
 120 thick silt and clay deposits with traces of sand that span about 10 meters (LSC). The silt
 121 is overlain with a silty-sand layer (2 m thick) that is followed by a fine sand layer that
 122 contains traces of clay (4 m thick). Since these two units are hydrostratigraphically
 123 similar, they are combined into a single hydrostratigraphic unit, Sd_l. Above unit Sd_l is a
 124 4.5-m-thick silt unit that contains layers of fine sand (SLS). This unit is followed by an
 125 8-m-thick layer of silty clay (USC). The upper 3 m of the site is composed of a sequence of

126 fine and medium sands that are overlain by a thin fine sand unit containing silt lenses. As
 127 with unit Sd_L, because this sequence of units displays similar hydrogeologic
 128 characteristics, they are combined into the hydrostratigraphic unit Sd_u. This unit is then
 129 being capped by a layer of clayey silt, which forms the modern surficial material (MS).
 130 extensive discussion of the site geology, hydrogeology, and geotechnical properties can
 131 be found in Germain (2019) and Diene (1989).

132 The water table on site is found about 2.1 m below the surface in the layer of fine to
 133 medium sand. The upper part of the sequence constitutes a shallow unconfined aquifer,
 134 while the fine sand layer found at depth (unit Sd_L, 18-24 m depth; Figure 3) can be
 135 considered a deep aquifer. Despite its depth, previous work has suggested that a phreatic
 136 water table may be present, as the sand layer was found to be only partially saturated at
 137 certain points in the year (Figure 3, unit SLS; Germain et al. *Submitted*).



139 Figure 3: Cross section showing site hydrogeology and the distribution of geologic
140 units between the field site (location A) and the far bank of the Sainte-Anne River
141 (location A')

142 The field site is located about 500 m away from the St. Anne River on level ground.
143 While the site was chosen because it is located far from the river and any important
144 topographic features, Germain et al. (submitted) demonstrated that seasonal river stage
145 variations influences pore water pressure at the site, due to a hydraulic connection within
146 the deep fine sand layer (unit S_{dL}).

147 **3 Methods**

148 **3.1 Piezometer installation methods**

149 The field site was instrumented with Geokon model 4500S vibrating-wire
150 piezometers. The piezometers were then connected to a datalogger (Geokon, LC-2 Series,
151 Model 8002-16) that converts the vibration frequencies measured by the instruments into
152 pore pressures through the use of a parabolic equation. The sampling rate for pore
153 pressure measurements was initially set to 12 hours from the period of December 2017 to
154 June 2018. The sampling rate was refined to 15 minutes for a pumping test (performed
155 between June 22 and August 6, 2018), as well as the entire fall of 2018. The rate was then
156 coarsened to 1 hour for the period from January 6, 2019 to the present.

157 The original set of piezometers installed on-site were individual piezometers in sand
158 packs (SP). In order to compare the performance of multilevel piezometers installed
159 using different methods, four multilevel piezometer nests were constructed using three
160 different methods: multilevel piezometers in sand packs (MLSP), and two different fully-

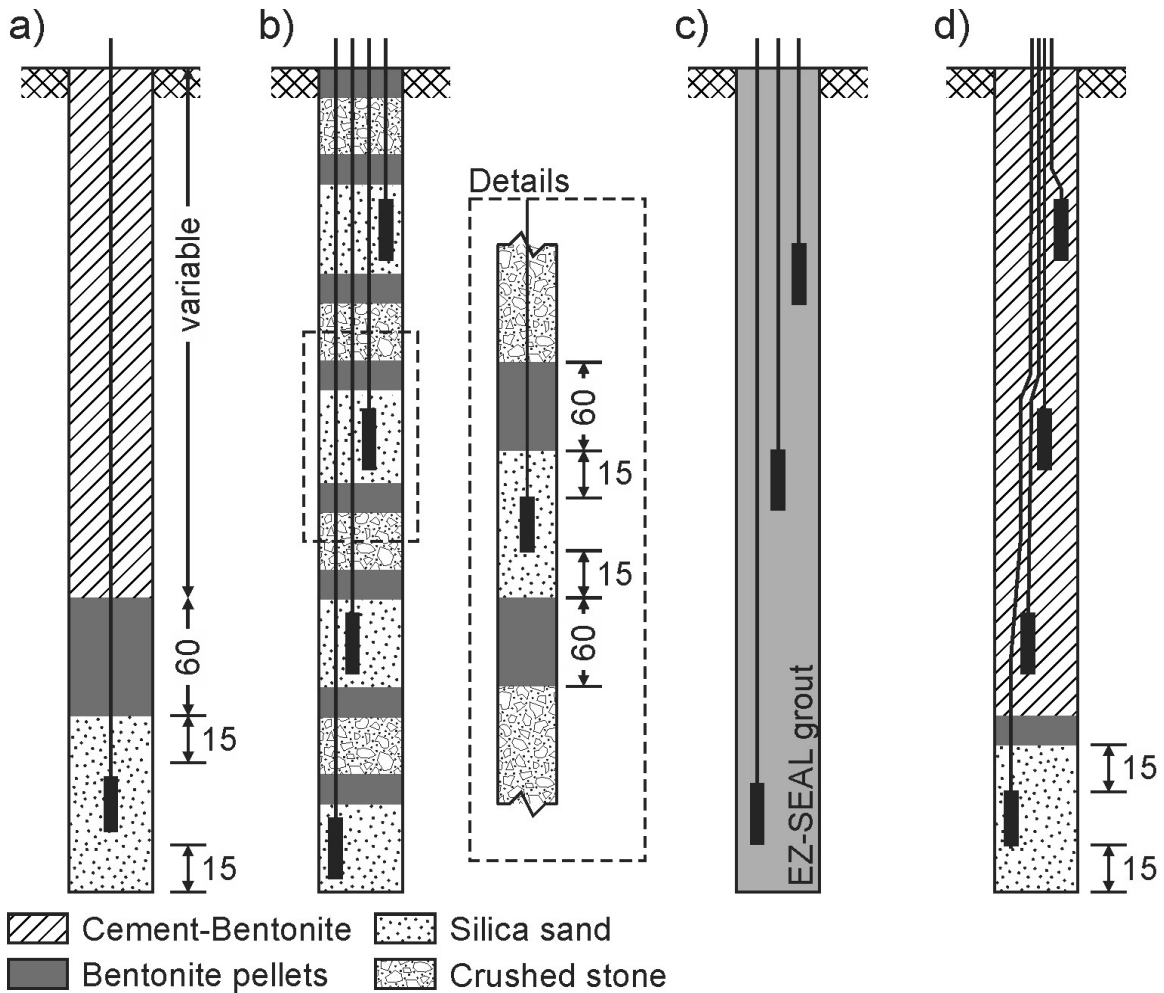
161 grouted methods: one using bentonite grout only (FGB) and one using a cement-bentonite
162 grout (FGCB). Data collected from the multilevel installations were then compared to
163 data gathered from the SP-type piezometers to assess similarity of performance.

164 **3.1.1 Individual piezometers sand packs**

165 This installation type consists of a single vibrating-wire piezometer installed in a sand
166 pack (SP) at the bottom of a borehole. The VWP is located in the middle of a 60 cm (2
167 foot) long sand pack made of industrial silica. The sand pack is overlain by a 60- cm-long
168 bentonite plug before the borehole was filled with a bentonite-cement grout (Figure 3a).
169 The grout used had water:cement:bentonite proportions of 5:1:1.25.

170 **3.1.2 Multilevel piezometers in sand packs (MLSP)**

171 This installation type consists of four multilevel vibrating-wire piezometers within a
172 single borehole. The VWPs are located in the middle of 60 cm (2 foot) long sand packs
173 made of industrial silica. The sand packs are underlain and overlain by a 60 cm-long
174 bentonite plug. Between the bentonite plugs, the borehole is filled with well-sorted
175 crushed stone (Figure 3b).



176

177 **Figure 3:** Schematic diagram of (a) a piezometer installed in a sand pack (SP), (b) a
 178 multilevel piezometer nest where each piezometer is installed in a sand pack (MLSP), (c)
 179 a fully-grouted piezometer nest within a single borehole (FGB), and (d) a cement-
 180 bentonite-grouted piezometer nest within a single borehole (FGCB). Length is in cm.

181 **3.1.3 Fully-grouted multilevel piezometers (bentonite grout; FGB)**

182 This installation type consists of four multilevel, fully-grouted, vibrating-wire
 183 piezometers within a single borehole. The grout is a mixture of granular bentonite (EZ-
 184 SEAL, Baroid Industrial Drilling Products) and water mixed at 20% solid content.
 185 According to the manufacturer datasheet, the typical hydraulic conductivity of this
 186 mixing ratio is 1×10^{-11} m/s. When installing these piezometers, the four VWP wires are
 187 attached using tie wraps, and then suspended at the desired depth in the open borehole,

188 within the drill rods. Then, the grout mixture is pumped from the bottom of the borehole
189 toward the surface, and the drill rods are progressively removed, leaving the piezometers
190 encased in grout (Figure 3c).

191 **3.1.4 Fully-grouted multilevel piezometers (cement-bentonite grout; FGCB)**

192 This type of installation is similar to the fully-grouted multilevel piezometers, except
193 that a mixture of cement and bentonite is used, and the bottom piezometer is located in a
194 sand pack instead of being fully grouted (Figure 3d). The sand pack is overlain by a 60-
195 cm-thick bentonite plug. The grout mixture used has water:cement:bentonite proportions
196 of 5:1:1.25, and using tables from Mikkelsen and Green (2003) the resulting mixture
197 would have a hydraulic conductivity of 6×10^{-9} m/s. Aside from these differences, the
198 installation is the same as the method detailed in Section 3.1.3.

199 **3.1.5 Installation depth**

200 The installation depths of the piezometers for each configuration is presented in Table
201 1 and Figure 2. Comparison of different configurations is made possible by instances
202 where piezometers of different arrangements are located at the same depths. For example,
203 at the depths of 8.5 m and 12 m, there is a piezometer in each of the three configurations,
204 and at 20-m-depth, there are piezometers in the FGB and MLSP configurations.

205 **Table 1:** Installation depths for each installation method, as well as the lithology of the
206 material containing each piezometer. Shaded cells indicate the depths where piezometers
207 were installed. Note that there are two different FGCB installations, while there is only
208 one installation each for the MLSP and FGB-type piezometers. Further note that for the
209 single piezometer, sand pack (SP) installation method, each shaded cell represents an
210 individual borehole. The hydrostratigraphic units referenced in Column 3 of the Table
211 correspond with those presented in Figure 2.

Installation depth (m)	Piezometer installation method				Instrumented material (hydrostratigraphic unit)
	SP	MLSP	FGB	FGCB	
2.8					Sand (S _u)
3.5					
4.35					Clay (U _{SC})
4.5					
8.5					
12					
20					Sand (S _L)
21					
25					Clay (L _{SC})
28					
32					
36					

212 Legend:

Installation Method:

SP Single piezometer in a sand pack

MLSP Multilevel piezometers with sand packs

FGB Fully-grouted multilevel piezometer with bentonite grout

FGCB Fully-grouted multilevel piezometer with cement-bentonite grout

Additional details:

	FGCB installation 1 (depths: 4.5m, 8.5m, 12m, 21m)
	FGCB installation 2 (depths: 25m, 28m, 32m, 36m)

213 **3.2 Barometric compensation**

214 Barometric compensation was applied to the VWP data in order to remove

215 atmospheric interference from the pore pressure data. This study utilizes the linear

216 method due to its relative simplicity and accurate results. According to this method, the
217 barometric compensation of measured VWP pore pressures is described by (Germain et
218 al. *Submitted*):

$$219 \quad u_t^* = u_t - LE(B_t - B_{ave}) \quad (1)$$

220 where u_t^* is the corrected pore pressure at time t , u_t is the measured pore pressure at time
221 t , LE is the loading efficiency, B_t is measured barometric pressure at time t and B_{ave} is the
222 average barometric pressure measured for the site. The loading efficiency correspond to
223 the fraction of barometric pressure that is transmitted to pore pressure through soil
224 compressibility, and is defined for undrained conditions as (Equation 1b):

$$225 \quad LE = \frac{m_v}{m_v + n\beta_w} \quad (1b)$$

226 where m_v is the soil vertical compressibility, n is the soil porosity and β_w is the water
227 compressibility. Practically, it is obtained from the ratio of pore pressure change to a
228 change in barometric pressure (Equation 1c):

$$229 \quad LE = \frac{\partial u_w}{\partial B} \quad (1c)$$

230 Following barometric compensation, the pore pressure was converted to hydraulic head
231 (m) by adding the pore pressure to the elevation of the VWP using the mean sea level
232 datum.

233 **3.3 Numerical modelling**

234 A 2-D, radial-coordinate numerical model was used to explore two questions, (1)
235 what is the impact of the grout permeability on transient head values in the piezometers,
236 and (2) can anomalies within the data could be explained by the presence of a hydraulic
237 short-circuit. The model extent is restricted to the silty clay unit (USC; 3-13 m depth)
238 where simple groundwater flow conditions were found (i.e., downward vertical flow).
239 Furthermore, because the sandy unit below unit USC (Sd_L) is partially-unsaturated and
240 hydraulically connected to the Sainte-Anne river, simulating the entire sediment sequence
241 would require the use of a significantly larger-scale model that includes the dynamics of
242 the river, which is beyond the scope of the present study (Germain et al., *submitted*).

243 Simulations of the groundwater flow were performed using the model
244 HydroGeoSphere (HGS; Therrien et al. 2006). For the conditions considered in this study
245 (fully-saturated conditions with transient water levels) this software simulates the flow of
246 groundwater using the control-volume, finite-element method. The general flow equation
247 solved by HGS is:

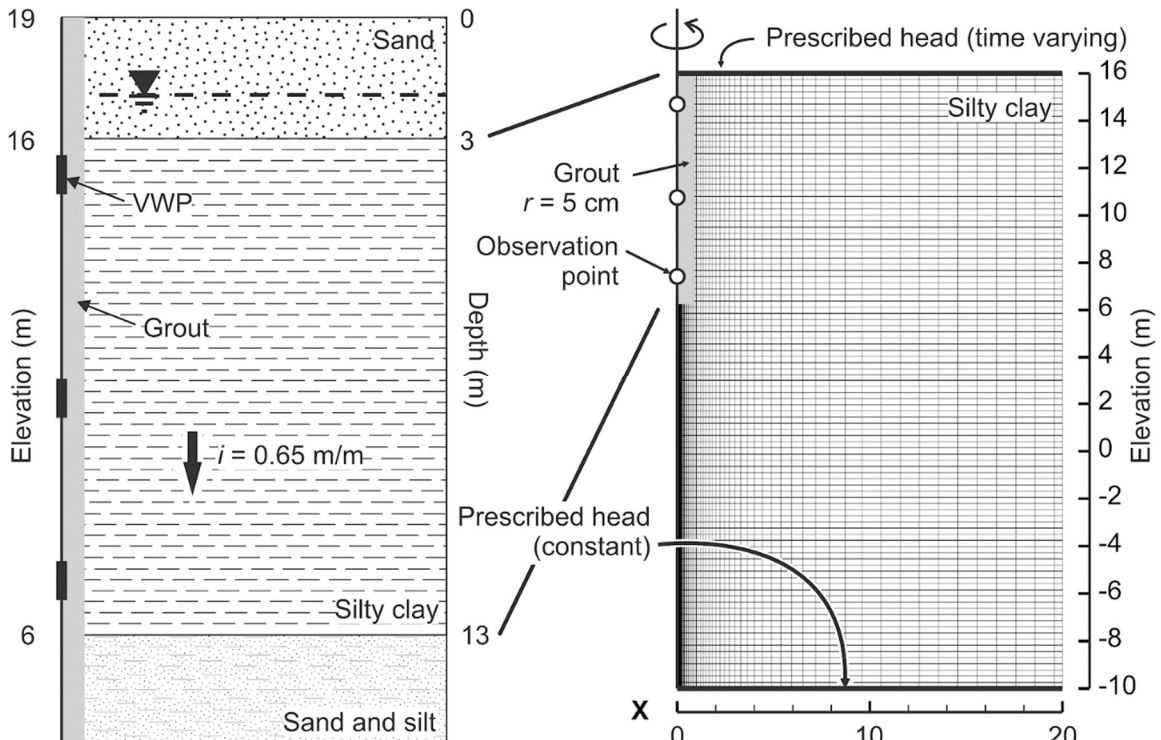
$$248 \quad K \frac{\partial^2 h}{\partial x^2} = S_s \frac{\partial h}{\partial t} \quad (2)$$

249 where K is hydraulic conductivity (m/s), h is hydraulic head, S_s is specific storage (m⁻¹),
250 and t is time (s). Given the geometry of the system under study, and for reasons of
251 numerical efficiency, this equation is solved in radial coordinates with axisymmetric
252 geometry.

253 Two sets of simulations were conducted. First, natural conditions (i.e., without a
254 grouted borehole) were simulated to obtain the theoretical transient head values within

255 the upper clay layer (USC; Figure 2) as influenced by head variations in the overlying
256 unconfined aquifer. Second, a borehole with a permeable grout was included in the clay
257 layer, and grout permeability was varied until a reasonable match was obtained with
258 observed heads. Note that no formal calibration exercise was performed, as the objective
259 was to test whether the excessively-permeable grout hypothesis can explain the
260 observations in the fully grouted piezometers.

261 The simulated vertical domain is 26 m long, with prescribed head boundaries at the
262 top and bottom of the model domain. The hydraulic head time series measured in a single
263 VWP located in the sand aquifer (Sd_u ; Figure 2) above unit USC is prescribed as a time-
264 varying boundary condition at the top boundary of the model, while the bottom boundary
265 is prescribed a constant head value of 0 m. This value was chosen in order to produce a
266 vertical downward gradient of about 0.65 m/m in the clay unit, as measured in the field.
267 While the actual thickness of the clay layer is 10 m, an additional 16 m of clay was
268 simulated in order to prevent the appearance of boundary effects in the simulated
269 piezometers (Fig. 4).



270

271

272

Figure 4. Conceptual model of the simulated domain, along with mesh and boundary conditions used for the numerical simulations.

273

274

275

276

277

278

279

280

281

282

283

284

The model has 60 horizontal elements, the width of which is refined from 1 m at the right boundary of the model, to 1 cm, near the well (left boundary). There are 260 vertical elements with a constant height of 10 cm, regardless of width. The hydraulic conductivity of the clay is considered isotropic with a value of 6.5×10^{-10} m/s, and the specific storage is $3.8 \times 10^{-5} \text{ m}^{-1}$ ($m_v = 3 \times 10^{-10} \text{ kPa}^{-1}$; Germain et al., *submitted*). These values were obtained using both permeability tests in a triaxial cell, and the interpretation of the effects of barometric variations on the hydraulic heads measured at the site. The grout material has a radius of 5 cm (2 in.) and a specific storage value similar to the clay was used. As mentioned above, the hydraulic conductivity was modified until a reasonable fit was obtained with the observed data. In order to do this, observation points were inserted in the model at 4.35, 8.5 and 12 m depth (model elevation of 14.65, 10.5 and 7 m respectively), which are the same depths as the piezometers in the FGCB installation.

285 **3.4 Events influencing hydraulic head measurements**

286 **3.4.1 Pumping test**

287 A pumping test was carried out on-site during the period from June 22 to August 6,
288 2018 at location 27215 (vertical shaded region, Figures 5-11). During this 45-day period,
289 the various slotted-screen piezometers at the study site and the vibrating-wire
290 piezometers at Location 27215 (Figure 1) were used as observation points. Consequently,
291 pumping associated with the test may have influenced the pressure measurements
292 recorded by the various piezometers on-site. However, the extent to which pumping may
293 have influenced measurements in an individual piezometer is highly dependent on the
294 horizontal and vertical distance from the pumping well. The highest impacts are expected
295 in the deep fine sand unit where the pumping well was located. Potential effects resulting
296 from the pumping test will be considered when comparing pore pressures for piezometers
297 located at the same depth, but installed in different configurations. Further details on the
298 pumping test can be found in Germain (2019).

299 **3.4.2 Grounding**

300 For the multilevel piezometer using sand packs (MLSP) and the fully-grouted
301 installation using bentonite-only grout (FGB), a pressure anomaly was observed
302 beginning June 1 at midnight until lasting until June 23, 2018. This anomaly was the
303 result of improperly-grounded dataloggers, which were influenced by a thunderstorm that
304 was present over the site from 6 p.m. to 7 p.m. on June 1, 2018 (denoted by a vertical
305 dashed line, Figure 5-11). Measurements returned to normal on June 23 after the
306 installation of a grounding wire. Thus, it is expected that the pressures measured by the

307 MLSP and FGB configurations will differ from those measured by the other piezometer
308 configurations for the aforementioned time period.

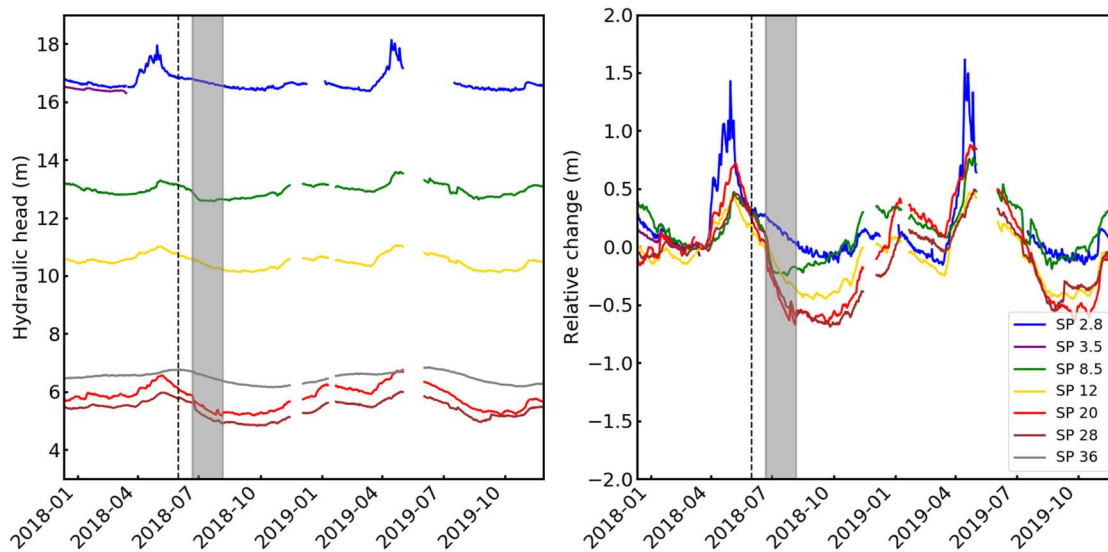
309 **4 Results**

310 The results are presented as follows: first, the hydraulic head values from the single
311 piezometers in sand packs (SP) are presented as a reference dataset that will be used
312 assess the performance of the multilevel installations. Next, the head profiles at
313 individual depths across all four types of installations are compared. The hydraulic head
314 profiles from all piezometers within a particular piezometer nest are then presented in
315 order to better identify any malfunctioning piezometers. Finally, results from the
316 numerical model are shown.

317 All results include differential head variations since the beginning of the monitoring
318 period in order to better compare the measured hydraulic head values between
319 installations. Additionally, all figures include water table variations measured with a
320 single VWP enclosed in a sand pack (referred to hereafter as SP_{2.8}), located within the
321 unconfined upper aquifer at 2.8 m depth. This head profile allows for comparisons to be
322 made between the dynamics of the water table in the unconfined aquifer and the head
323 profiles measured by each of the piezometer nests. Note that all figures highlight the
324 presence of the thunderstorm (vertical dashed line, Figures 5-11) and the pressure
325 anomaly (vertical shaded region, Figures 5-11) caused by the pumping test as described
326 in Section 3.4.1.

327 **4.1 Reference dataset: individual piezometers in a sand pack (SP)**

328 While not a true piezometer nest, piezometers of the same construction located at
329 different depths can be superimposed to detect possible measurement anomalies in the
330 multilevel installations. When plotted together, data from the SP-type piezometers show
331 that increases in hydraulic head during the spring recharge event are largest near the
332 surface, and then progressively dampen with depth (Figure 5, left panel).



333

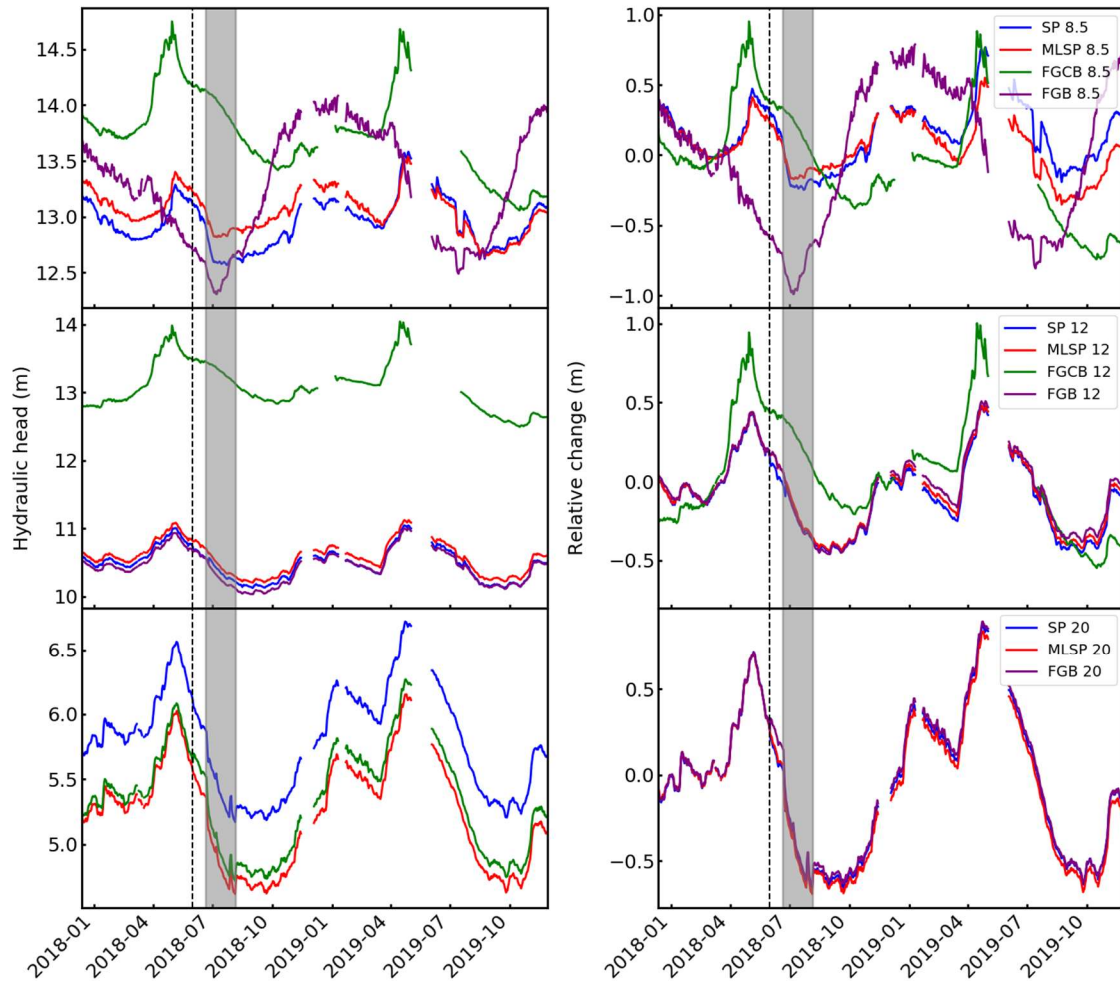
334 **Figure 5.** Hydraulic head profiles (left panel), and observed changes in hydraulic head
335 (right panel) for 2018 and 2019 measured by the individual piezometers with sand packs.
336 Note that the data from SP_{3.5} (purple line) were omitted after April, 2018 due to a
337 malfunction in the piezometer.

338 There is also an observable phase lag in the hydraulic head peaks which becomes more
339 pronounced with depth (Figure 5, right panel). Interestingly, the amplitude of the increase
340 for SP₂₀ remains higher than that of SP₁₂ and SP_{8.5}, indicating that vertical infiltration is
341 not the only process influencing changes in hydraulic head within the piezometers.

342

343 **4.2 Comparison of head variations in piezometers at the same depth across**
344 **different installations**

345 In all piezometers, regardless of depth or installation method, there is an increase in
346 hydraulic head which occurs towards the end of March/beginning of April, before
347 reaching a maximum in late April/early May (Figure 6). This increase in head
348 corresponds with the spring snowmelt, which is the largest annual groundwater recharge
349 event in this area. Maximum head values are followed by a recession period that
350 continues until the fall, where slight increases in hydraulic head are observed. The effect
351 of the pumping test is only observed in piezometers located within units Sd_L or LSC, at
352 depths of 20m and deeper (Figure 6, third row). Similarly, the effect of the electrical
353 storm can also be observed (e.g., MLSP at a depth of 12m; Figure 6, second row; and
354 FGB piezometers at a depth 20 m, Figure 6, third row).



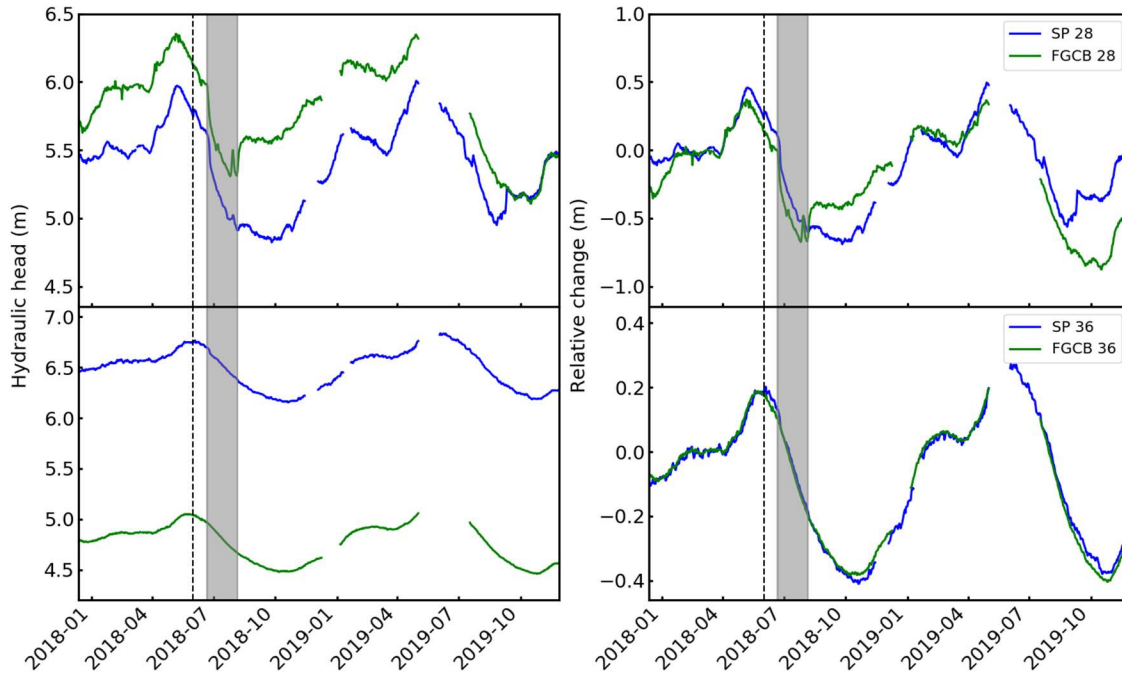
355

356 **Figure 6:** Hydraulic head profiles (left) and the change in hydraulic head values (right)
 357 for piezometers at depths of 8.5m, 12 m, and 20 m (first-third rows, respectively).

358 At 8.5 m (Figure 6, first row), the piezometers with sand packs show markedly
 359 different responses when compared with the fully-grouted methods. For instance, the
 360 spring rise in head (derived from snowmelt at the end of March) is not felt by the FGB_{8.5}
 361 piezometer (Figure 6, first row, green line). Additionally, the hydraulic head values
 362 measured by the FGCB-type piezometer, are about 0.5 m higher than those observed in
 363 the sand-pack type piezometers, MLSP_{8.5} and SP_{8.5}. Furthermore, FGCB_{8.5} has a larger
 364 increase in hydraulic head in the spring when compared with all other installation
 365 methods, and the shape of the head profile is significantly different.

366 At 12 m (Figure 6, second row), large differences (up to 2 m for hydraulic head and
367 0.5 m for the change in head) are observed in the FGCB₁₂, while the responses are
368 smaller in the three other arrangements. The head profiles and change in head curves are
369 almost perfectly superimposed for FGB₁₂, MLSP₁₂, and the SP installation. The curves
370 for FGB₁₂ and MLSP₁₂ show the influence of the thunderstorm on June 1, 2018, as head
371 variation curves between a difference of approximately 0.1 m until the grounding pins
372 were installed four weeks later.

373 At 20 m (Figure 6, third row), the head profile curves have similar shapes, but the
374 values measured differ by between 0.2 and 0.5 m across the three installation types that
375 were present. In addition, a sudden increase in head occurs from June 2 in the FG₂₀
376 piezometer, at the time of the thunderstorm. This increase dissipates on June 22, 2018 at
377 the start of the pumping test. The relative head change curves for the three installations
378 are almost identical.



379

380 **Figure 7:** Barometrically-compensated hydraulic head values (left) and the change in
 381 head (right) for the piezometers at depths of 28 m and 36 m.

382 At 28 m (Figure 7, first row), the head profiles have a generally similar shape, but
 383 with notable differences in June 2018, likely due to the pumping test. Otherwise, the two
 384 piezometers display a difference of approximately 0.7 m throughout the period studied,
 385 despite a difference in elevation of only 0.1 m (Table 1). The curves for the relative
 386 change in head are also roughly similar, however the hydraulic head peaks of March and
 387 May reach a different magnitude and are slightly offset in time.

388 At 36 m, the head profiles have a very similar shape, but there is a difference in head
 389 of about 1.7 m between the two piezometers (Figure 7, second row). This is a large
 390 deviation given the difference in elevation between the two piezometer installations is
 391 about 0.1 m (Table 1). On the other hand, the curves showing the changes in hydraulic
 392 head are very similar, the head peaks have the same magnitude, and there is no apparent

393 time lag, which means both installations react identically to the spring recharge event. A
394 slight increase in head for the piezometer SP₃₆ can be observed in the relative change
395 curves following the electrical storm, but this variation is small, and is eventually muted
396 by the start of the pumping test (Figure 7, right panel). Since there were no co-located
397 FGB or MLSP piezometers below 20 m depth, the comparative performance of the deep
398 FGCB installation was not able to be assessed.

399 **4.3 Hydraulic head variations in piezometer nests using three different** 400 **construction methods**

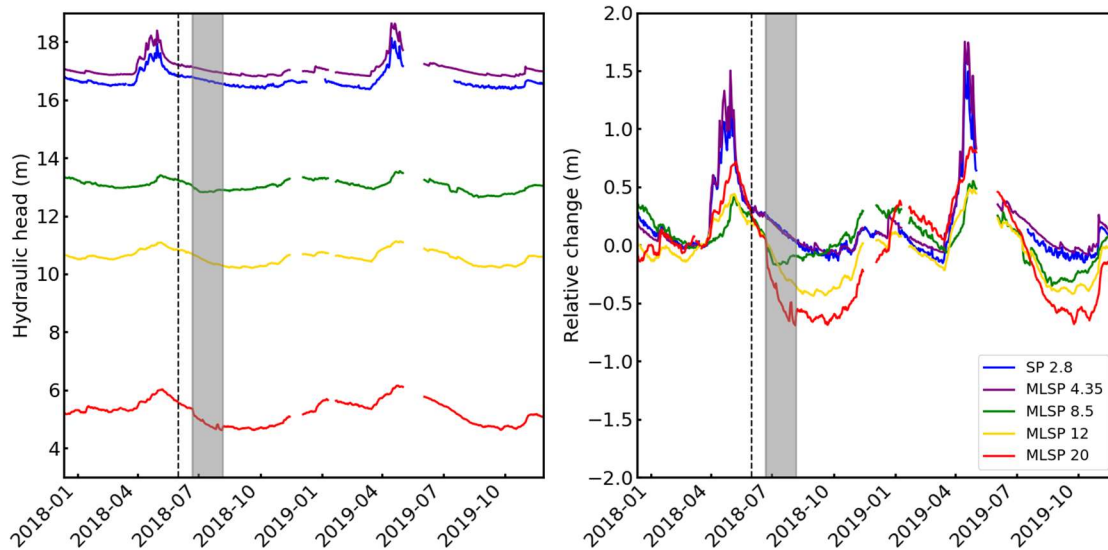
401 Hydraulic head profiles for all piezometers in each type of installation were
402 compared to both assess piezometer performance relative to the head changes in the
403 surficial aquifer, and detect the presence of any hydraulic short circuits in a piezometer
404 nest. Operating under the initial assumption that groundwater at the study site is
405 exclusively vertical, it is expected that the head variations in each piezometer nest are
406 related to the head variations in the surficial aquifer, as measured by well SP_{2.8}.

407 **4.3.1 Multilevel piezometers with sand packs (MLSP)**

408 Data from all of the piezometers within the MLSP installation show an increase in
409 hydraulic head resulting from the spring recharge event, regardless of depth. There are,
410 however, variations in the magnitude of the change in head to this event. The data show
411 that the hydraulic head peaks in MLSP_{4.35} are slightly higher than those observed in the
412 surficial aquifer (MLSP_{4.35} and SP_{2.8}; Figure 8). Since this scenario is not physically
413 possible, the differences are quite small, and the wells are approximately co-located (~10

414 m apart), such results are likely the product of measurement uncertainty in either the
415 depth or barometric measurements.

416



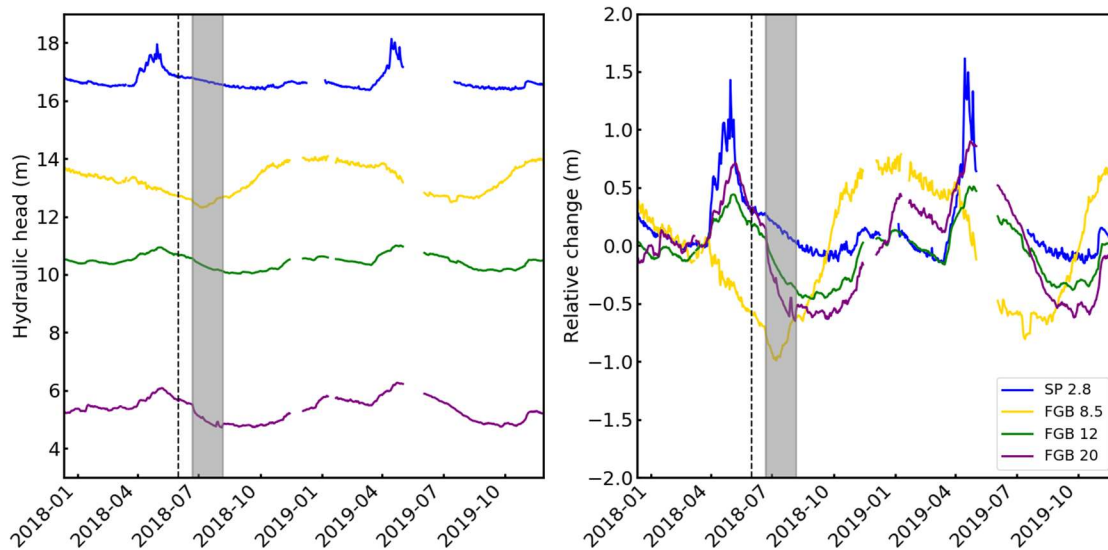
417

418 **Figure 8.** Hydraulic head profiles (left panel) and observed changes in hydraulic head
419 (right panel) for 2018 and 2019 in the piezometer nest that utilized multi-level
420 piezometers with sand packs. The observed changes in hydraulic head in the upper
421 aquifer (SP_{2.8}; blue line) are included for comparison.

422 When the data from the MLSP installation are compared with the hydraulic heads in
423 the surface aquifer (SP_{2.8}), the shape of the head profiles for the MLSP-type piezometers
424 are similar to that of the surface water table, but with the high-frequency events filtered
425 out. Furthermore, the amplitude of the hydraulic head changes progressively decreases
426 with depth. The timing of the hydraulic head peak in MLSP_{4.35} is synchronous with that
427 of the surficial aquifer. For the deeper piezometers, the hydraulic head peaks are still
428 fairly synchronous, however there is an 8-day phase lag between these piezometers and
429 MLSP_{4.35}/ SP_{2.8}.

430 4.3.2 Fully-grouted piezometers with bentonite grout (FGB)

431 Comparing the responses of the different piezometers within a single FGB installation
432 reveals a number of notable differences compared to the MLSP reference dataset. (Figure
433 9).



434

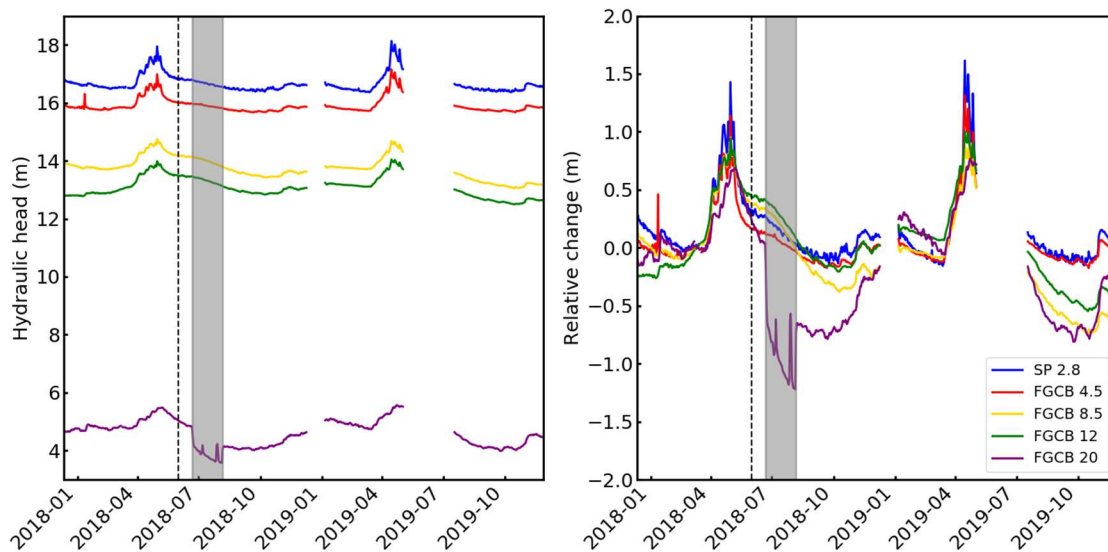
435 **Figure 9.** Hydraulic head profiles (left panel) and observed changes in hydraulic head for
436 2018 and 2019 (right panel) in a fully-grouted piezometer nest using bentonite grout
437 (FGB). Hydraulic head changes in the surficial aquifer above are shown for reference
438 (SP_{2.8}).

439 The most prominent observation is that the hydraulic head profile of the FGB_{8.5}
440 piezometer does not show any response to the spring recharge event (Figure 9, left panel,
441 yellow line). Additionally, piezometers FGB₁₂ and FGB₂₀ exhibit responses similar to the
442 head fluctuations in the surficial aquifer (Figure 9 right panel, green and purple lines,
443 respectively), though the high frequency events are largely filtered out. There is a small
444 (~ 3 day) time lag between the peak water level observed by the FGB piezometers and
445 those observed by the reference well. The peak for FGB₁₂ arrives approximately 3 days
446 earlier than that observed in FGB₂₀, however, the increase in hydraulic head that occurs

447 in response to the spring recharge event is higher for FGB₂₀ than for FGB₁₂. This
448 difference is significant, as the opposite would be expected if the increase in head was
449 due solely to vertical water infiltration from the surface.

450 4.3.3 Cement-bentonite-grouted multilevel piezometers (FGCB)

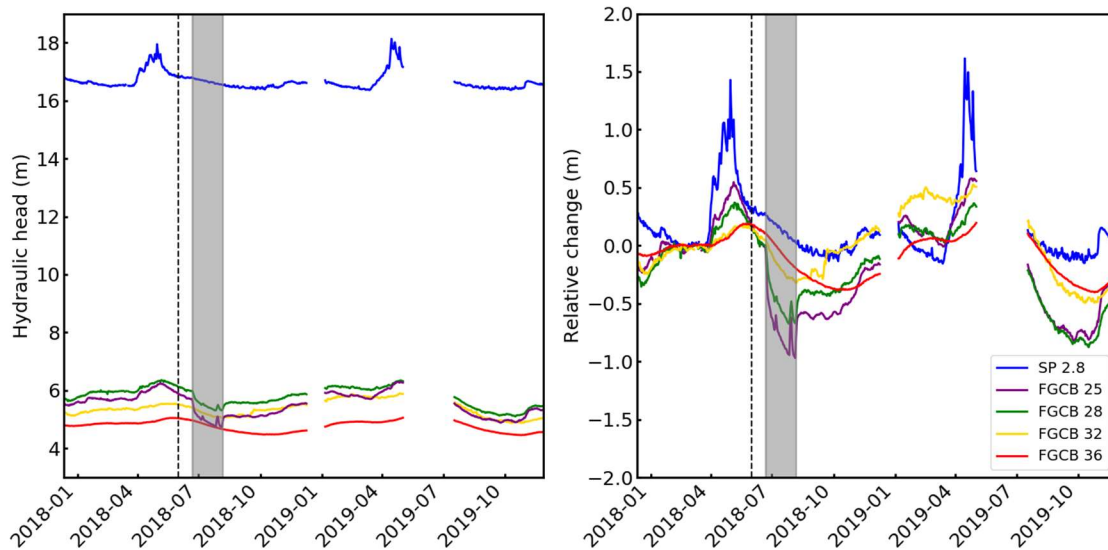
451 There are two FGCB installations, one shallow (4.5-21 m depth) and one deep (25-36
452 m depth). For the shallow nest, the hydraulic head profiles of the three piezometers are
453 located in the upper silty clay layer (unit USC; Figure 2). These piezometers, FGCB_{4.5},
454 FGCB_{8.5}, and FGCB₁₂, respectively, have shapes that are very similar to that of the
455 piezometer located in the surficial aquifer (Figure 10, right panel). Furthermore, the
456 amplitude of the head variations in response to the spring recharge event are similar for
457 these three piezometers, though the effect dampens with depth. The apparent
458 synchronization of the peak head values further demonstrates the similar behavior of
459 these three piezometers (Figure 10, left panel).



461 **Figure 10.** Hydraulic heads (left panel) and observed change in hydraulic head for 2018
462 and 2019 in the shallow, fully-grouted piezometers using cement-bentonite grout
463 (FGCB). The observed changes in hydraulic head within a piezometer in the upper
464 aquifer (SP_{2.8}; blue line) is included for comparison.

465 The behavior of piezometer FGCB₂₁, located in the intermediate fine sand layer (S_{dL};
466 Figure 2) is similar to that of the aquifer in the surface aquifer, but it does not have the
467 same peaks in the head profile as seen in FGCB_{4.5} and FGCB_{8.5}. The amplitude and date
468 of the head change peak are noticeably different compared to the other three piezometers,
469 as the amplitude of the peak is smaller and it occurs out of phase with the other peaks by
470 about 6 days. Most notably, FGCB₂₁ is the only piezometer that exhibits changes in head
471 during the pumping test.

472 The deep FGCB nest is located within the deeper layer of clay silt (LSC) and till (T;
473 Figure 2). Unlike the shallow FGCB nest, there is substantial time lag in the observed
474 head peaks between the shallowest piezometer in the nest, at 25 m depth, and the deepest
475 (36 m depth). There is also a marked attenuation of the amplitude of the head profiles
476 (Fig. 11, left panel)



478

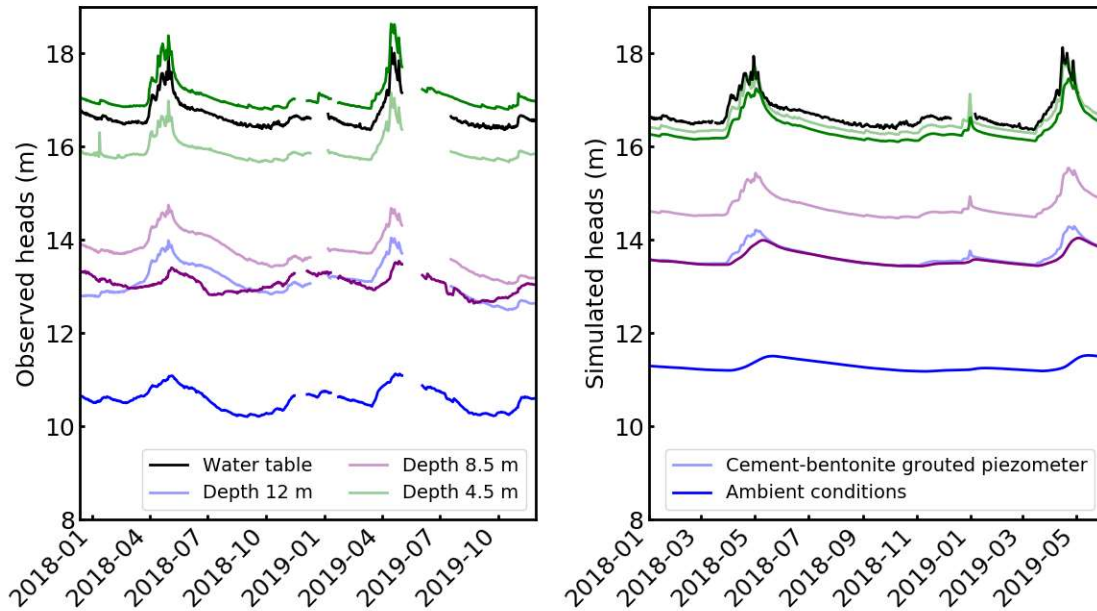
479 **Figure 11.** Hydraulic head profiles (left panel) and observed changes in hydraulic head
 480 (right panel) in the deep fully-grouted piezometer nest using cement-bentonite grout for
 481 2018 and 2019. The observed head changes for a piezometer in the upper aquifer (SP_{2.8};
 482 blue line) are included for comparison.

483 The head profiles also have a smoother shape with respect to the profile of the
 484 reference well. The phase lag between head peaks increases with the depth from the
 485 surface, up to a maximum of 25 days, as observed in FGCB₃₆ in 2018. It should also be
 486 noted that the pumping test has a marked effect on the head profiles from the piezometers
 487 at 25, 28, and 32 m.

488 4.3 Numerical results

489 Hydraulic heads were simulated at depths of 4.35, 8.5 and 12 m, for undisturbed
 490 conditions (dark lines; Figure 12, right panel), and after the installation of a fully-grouted
 491 piezometer where the grout hydraulic conductivity 500 times higher than that of the
 492 surrounding clay (pale lines; Figure 12, right panel). The modeling results are then

493 compared with observations at the same depths made with FGCB (pale lines; left panel)
494 and SP-type piezometers (dark lines; left panel).



495
496 **Figure 12.** Observed vibrating-wire piezometer data for installations using sand packs
497 (dark lines) and fully-grouted methods (pale lines). Simulated hydraulic heads for
498 ambient conditions (i.e., no piezometer; dark line) and in a FGCB piezometer.

499 Model results show that the simulated ambient conditions are similar to the observed
500 head profiles in the SP-type piezometers. Meanwhile, when highly permeable grout is
501 used to simulate the effects of a hydraulic short circuit, model results strongly resemble
502 the observed head profiles from the FGCB-type piezometers. In these profiles, high
503 frequency variations quite visible and heads values are higher than those observed under
504 ambient conditions. These results suggest that the SP-type piezometers located on site are
505 functioning properly and the observed head profiles from these installations can be
506 considered largely representative of undisturbed conditions. They also suggest that the
507 observations from the FGCB installation correspond to a hydraulic short circuit, resulting

508 in an effective permeability around the piezometer which is almost 500 times that of the
509 host formation.

510 **5 Discussion**

511 The fully-grouted installation method has received considerable support in current
512 geotechnical and hydraulic engineering literature (Marefat et al. 2018; Marefat et al.
513 2017; Smith et al. 2013; Simoni, 2012). However, there are currently no standard
514 methods for proper installation of fully-grouted piezometers (e.g., ASTM guidelines).
515 Furthermore, data from both piezometer nests using a form of fully-grouted installation
516 indicate that some of the piezometers may not be functioning properly.

517 The majority of piezometers recorded a signal compatible with the hydrogeological
518 context, regardless of installation method. These piezometers recorded an episode of
519 significant spring recharge, followed by a period of summer recession. A second recharge
520 episode occurs in the fall, which is then followed by a winter recession. There were,
521 however, a few piezometers that exhibited obvious malfunctions when compared with
522 other piezometers at similar depth, or when compared with expected hydraulic
523 head/pressure curves for the hydrogeologic context. Data indicate that two specific
524 piezometers are not functioning correctly, and that an entire FGCB piezometer
525 installation appears to be malfunctioning.

526 **5.1 Identifying malfunctioning piezometers**

527 Within the FGB piezometer nest, FGB_{8.5} exhibits a very different hydraulic head
528 curve from the other piezometers in the installation (Figure 10). Furthermore, the

529 response of this piezometer is incompatible with the hydrogeological context, as the rate
530 of change in hydraulic head is much greater than that measured in other types of
531 piezometers located at the same depth (Figure 6, first row).

532 While there was evidence that an individual piezometer within the FGB may be
533 recording anomalous values, it appears that the entire FGCB installation is not
534 functioning properly. As shown in Fig. 8, the head values measured at 8.5 and 12 m were
535 1 to 2 m higher than those measured by other piezometers at the same depth but installed
536 with different methods. In addition, the hydraulic head curves from these two
537 piezometers, as well as the piezometer located at 4.5m, were practically identical to that
538 measured in the surface aquifer. These observations are indicative of a hydraulic short
539 circuit (McKenna, 1995). However, in this string of FGCB piezometers, the deepest
540 piezometer does not seem to exhibit the same problems, probably due to the fact that it is
541 located in a permeable unit and that it is enclosed in a sand pack.

542 There are two hypotheses that could explain the hydraulic short circuit observed in
543 the FGCB piezometer nest. The first posits that there is an issue with the permeability of
544 the bentonite-cement grout. Based on the work of Marefat et al. (2017), the theoretical
545 vertical hydraulic conductivity value calculated for the grout from the water-cement-
546 bentonite proportions (water = 5 portions, c = 1 portion, b = 1.25 portion) used on the site
547 gives approximately 6×10^{-9} m/s. This value is an order of magnitude greater than that of
548 the vertical hydraulic conductivity of the clay layer measured in the laboratory (6×10^{-10}
549 m/s; Germain et al. *submitted*). According to Marefat et al. (2019), hydraulic short
550 circuits occur when the hydraulic conductivity of the grout is two orders of magnitude
551 higher than that of the geological formation. Thus, at our field site, it is unlikely that the

552 short circuit resulted from excessively permeable grout. However, it should be noted that
553 the calculation of the hydraulic conductivity is an estimate based on the proportions used
554 to prepare the grout, which are approximate.

555 The second explanation concerns the existence of a preferential flow path between
556 instruments created during installation. This preferential pathway can exist along the
557 space between the sheath cables, or it can result from a space between the grout and the
558 formation due to excessive shrinkage during curing. While the presence of such features
559 can indicate installation error, preferential flow paths have also been reported in studies
560 where great care was taken to ensure proper installation (Wan and Standing
561 2014). Indeed, many studies suggest using a grout pipe with the VWP attached radially
562 outside the pipe, while here, a suspended bundle was used. Depending on the grout
563 viscosity, the space between the cables may have not been filled and cause a preferential
564 pathway. While Marefat et al. (2018) observed grout shrinkage of samples after partially
565 curing under atmospheric conditions, it is less likely to happen at depth where saturated
566 conditions are present.

567 While the exact cause is unknown, the preferential flow path hypothesis fits the
568 observations presented in Figure 7, where the hydraulic head curves for FGCB_{4,5},
569 FGCB_{8,5}, and FGCB₁₂ vary synchronously and with the same amplitude as the surface
570 aquifer. Indeed, if the grout was of appropriate permeability and did not contain a
571 preferential path, the energy loss associated with the downward flow of groundwater
572 would result in both a time lag and reduction in amplitude of the hydraulic head peaks,
573 like shown with the numerical model. This behavior is documented by Marefat et al.
574 (2019), which shows that the signal recorded by a piezometer 22 m deep installed in a

575 grout similar to the surrounding geology is out of phase by several days, even several
576 weeks, compared to the surface signal. In addition, it shows that during a hydraulic short
577 circuit due to the permeability of the grout, there is still a decrease in the amplitude of the
578 signal by about 0.2 m (Marefat et al., 2019).

579 **5.2 Suggestions for future installations in Champlain clay-type deposits**

580 Analysis of the different piezometer nests at the Sainte-Anne-de-la-Pérade site shows
581 that the multilevel piezometers with sand packs (MLSP) and the fully-grouted piezometer
582 nests sealed with bentonite (FGB) installation methods are the most reliable for use in
583 massive clay deposits. This determination is based on the fact that piezometers installed
584 at the same depth with these arrangements recorded similar variations in hydraulic head.
585 While some piezometers within individual installations were found to not be functioning
586 properly, these issues were likely due to instrument problems as opposed to a
587 fundamental issue with the installation method. Furthermore, while one string of the
588 cement-bentonite-grouted piezometers (FGCB) appeared to function properly, the
589 hydraulic short circuit detected in the second string (likely due to a grout-related issue)
590 suggests that using this method introduces an unnecessary degree of risk to the long-term
591 functionality of a given piezometer installation. The increased risk of failure largely
592 stems from a lack of standard methods concerning both the construction of fully-grouted
593 piezometers and the mixture of cement-bentonite grout.

594 While some fully-grouted piezometers used in this study worked correctly, the lack of
595 a standard method is concerning. Consulting different studies yields a number of different
596 installation methods, however there is not significant documentation on how these

597 methods may influence piezometer performance and the presence of comparative studies
598 on the topic is limited (Mickelsen and Green 2003; Contreras et al. 2012; Marefat et al.
599 2018). Furthermore, while there are a number of different given “recipes” and guidelines
600 for mixing cement bentonite grout, many of these methods employ subjective or
601 qualitative descriptors for the recommended grout consistency (Mickelson 2002; Marefat
602 et al. 2018). Thus, because of the lack of guidance for both construction and grout
603 preparation, using bentonite grout removes a degree of subjectivity from the construction
604 process, thereby potentially reducing the risk of piezometer failure resulting from
605 construction error. Furthermore, there is evidence that cement-bentonite grout may
606 interact with some types of VWP filters, which may ultimately render this type of grout
607 inadvisable for use in low-permeability formations (Simonsen and Sorenson, 2018).

608 The MLSP method performed well, and installations using sand packs have
609 traditionally been used by the Quebec Department of Transport to monitor hydraulic
610 heads/pore pressures within clayey slopes. There is also extensive documentation from
611 both governmental and academic sources which demonstrate the continued successful
612 performance of these methods (Lafleur et al., 1988; Chapuis et al. 2012; Germain et al.
613 *Submitted*) As such, these installations can be considered adequate and should be used in
614 the future. However, we would recommend using bentonite instead of crushed stones
615 between the bentonite plugs. Yet the fact that the fully grouted piezometers (particularly
616 those using cement-bentonite grout) performed less well should not be interpreted as a
617 need to abandon the use of this installation method when building infrastructure for
618 monitoring clay slopes across the province. The FGB-type layout has two main
619 advantages over “conventional” installation methods: ease and speed of installation

620 (McKenna, 1995; Mikkelsen, 2002). Furthermore, the fact that FGB-type installations
621 can use either one or multiple piezometers within a single borehole filled with a single
622 material (grout) results in a cost-efficient installation method that can instrument a large
623 area both laterally as well as vertically. However, the relative lack of guidance on the
624 proper implementation of this technique means that it must be undertaken with
625 considerable care, particularly if cement-bentonite grout method is used.

626 **5.3 Continuing work and directions for future research**

627 A series of laboratory investigations were started in the fall of 2019 in order to
628 provide additional guidance when using cement-bentonite grout. These experiments,
629 which are still ongoing as of April, 2020, seek to measure the hydraulic conductivity,
630 viscosity, and shrinkage of grout mixtures when different proportions of cement and
631 bentonite are used. While laboratory experiments can help to assess grout performance,
632 additional piezometer installations using fully-grouted methods (using both bentonite and
633 cement bentonite grouts) are also recommended. These additional installations can be
634 used to better document the performance of specific fully-grouted installation methods
635 with regards to piezometer performance and the rate of installation-related malfunctions.
636 Additionally, a long-term monitoring study is recommended to compare the performance
637 of FGB-type piezometers with sand-pack-type piezometers over extended time periods.

638 **6 Conclusion**

639 This study assessed the performance of different methods for installing multilevel
640 vibrating wire piezometers at a field site in the municipality of Sainte-Anne-de-la-Pérade

641 that possessed a complex stratigraphy. Comparison of the three different installation
642 methods showed the use of sand packs or bentonite grout resulted in similar performance.
643 Of the two fully-grouted installations using cement-bentonite grout, one installation
644 failed completely due to a hydraulic short circuit. This short circuit is likely the result of
645 either shrinkage of the grout, or flow occurring along the wires of the instruments.

646 While the bentonite-grouted piezometers used in this study worked correctly, the
647 absence of a standard method for installation is concerning. A review of the literature
648 provides a number of different installation methods, as well as a number of different
649 recipes for mixing cement-bentonite grout—many of which contained a number of
650 subjective or qualitative descriptions. Thus, due to the lack of guidance for both
651 construction and grout preparation, the use of a bentonite grout will likely remove a
652 degree of uncertainty when fully-grouted installation techniques are used. However, the
653 fact that the fully grouted piezometers using cement-bentonite grout performed less well
654 does not mean that all fully-grouted methods should be avoided. The relative ease, speed
655 of installation, cost efficiency of these types of piezometers means that they can be used
656 to instrument a large area, both laterally as well as vertically.

657 **7 Acknowledgements**

658 This work was funded by the Quebec Ministry of Public Security through the 2013-
659 2020 Action Plan on Climate Change (PACC 2013-2020) and the Québec Government's
660 Green Fund.

661 **8 References**

662 Anochikwa, C.I., van der Kamp, G., and Barbour, S.L., 2011. "Interpreting pore-water
663 pressure changes induced by water table fluctuations and mechanical loading due to
664 soil moisture changes." *Can. Geotech. J.*, 49, 357-366.
665

666 Cloutier, C., Locat P., Demers, D., Fortin, A., Locat, J., Leroueil, S., Locat, A., Lemieux,
667 J.-M. and Bilodeau, C. (2017). "Chapter 47 – Development of a long term monitoring
668 network of sensitive clay slopes in Québec in the context of climate change.
669 Landslides in sensitive clays", *Advances in natural and technological hazards
670 research* 46, pp. 549-558. Springer International Publishing.
671

672 Contreras, I. A., Grosser, A. T., and VerStrate, R. H. 2008. "The use of the fully-grouted
673 method for piezometer installation." *Geotech. Ins. News*, 26, 30-37.
674

675 Contreras, I. A., Grosser, A. T., and VerStrate, R. H. 2012. "Update of the fully-grouted
676 method for piezometer installation." *Geotech. Ins. News*, 30(2), 20–25.
677

678 Demers D., Robitaille D., Locat P., Potvin J. 2014. "Inventory of Large Landslides in
679 Sensitive Clay in the Province of Québec, Canada: Preliminary Analysis." In:
680 L'Heureux JS., Locat A., Leroueil S., Demers D., Locat J. (eds) *Landslides in
681 Sensitive Clays. Advances in Natural and Technological Hazards Research*, vol 36.
682 Springer, Dordrecht
683

684 Germain, A. 2019. "Étude de l'infiltration et des variations verticales de la pression
685 interstitielle dans un massif argileux" [in French]. M.Sc. Thesis. Université Laval.
686 <http://hdl.handle.net/20.500.11794/37220>
687

688 Germain, A., N.L. Young, J-M. Lemieux, H. Delottier, A. Locat, and Mony, L. In
689 Preparation. "Hydrogeology of a complex Champlain Sea deposit (Quebec, Canada):
690 Implications for slope stability." Currently in preparation for submission to *Canadian
691 Geotechnical Journal*.
692

693 Lafleur, J., Silvestri, V., Asselin, R., and Soul, M. 1988. "Behaviour of a test excavation
694 in soft Champlain Sea clay." *Can. Geotech. J.* 25, 705-715
695

696 McKenna, G.T., 1995. "Grouted-in installation of piezometers in boreholes." *Can.
697 Geotech. J.*, 32 (2), 355-363.
698

699 Mikkelsen P.E., 2002. "Cement–bentonite grout backfill for borehole instruments."
700 *Geotech. News* 20 (4), 38–42.
701

702 Mikkelsen, P.E. and Green, G.E., 2003. "Piezometers in fully grouted boreholes."
703 FMGM-field measurements in geomechanics, Oslo, Norway.
704

705 Merefat V., Duhaime F., Chapuis R., 2015. "Pore pressure response to barometric
706 pressure change in Champlain clay: Prediction of the clay elastic properties." *Eng.
707 Geo.*, 198, 16-29.

708

709 Marefat, V., Duhaime, F., Chapuis, R.P. and Le Borgne, V., 2017. "Fully grouted
710 piezometers in a soft Champlain clay deposit - Part I: Piezometer installation."
711 Geotech. News. 35(3): 35-38

712

713 Marefat, V., Duhaime, F., Chapuis, R.P. and Le Borgne, V., 2018. "Performance of fully
714 grouted piezometers under transient flow conditions: Field study and numerical
715 results." Geotech. Testing J., 42(2).

716

717 Obbink, J.G. 1969. "Construction of piezometers, and method of installation for ground
718 water observations in aquifers." J. Hydro., 7, 434-443.

719

720 Simeoni, L. 2012. "Laboratory tests for measuring the time-lag of fully grouted
721 piezometers." J. Hydro., 438-439, 215-222.

722

723 Simonsen, T.R., and Sorensen, K.K. 2018. Performance Of Vibrating Wire Piezometers
724 In Very Low Permeable Clay. Proceedings of the International Symposium on Field
725 Measurements in Geomechanics 2018.

726

727 Smith, L.A., van der Kamp, G., and Hendry, M.J. 2013. "A new technique for obtaining
728 high-resolution pore pressure records in thick claystone aquitards and its use to
729 determine in situ compressibility." Wat. Res. Research 49(2), 732-743.

730

731 Therrien, R., R. McLaren, E. A. Sudicky, and Panday, S. 2006, "HydroGeoSphere—A
732 Three-Dimensional Numerical Model Describing Fully-Integrated Subsurface and
733 Surface Flow and Solute Transport." Groundwater Simul. Group, Waterloo, Ont.,
734 Canada.

735

736 Van der Kamp, G. 2001. "Methods for determining the in situ hydraulic conductivity of
737 shallow aquitards — an overview." Hydrogeol. J. 9, 5–16.

738

739 Wan, M.S.P., and Standing, J.R. 2014. "Field measurement by fully grouted vibrating
740 wire piezometers." Proceedings of the Institution of Civil Engineers.
741 <http://dx.doi.org/10.1680/geng.13.00153>